View metadata, citation and similar papers at core.ac.uk

brought to you by CORE

provided by RERO DOC Digital Library

Mon. Not. R. Astron. Soc. **369,** 257–271 (2006) doi:10.1111/j.1365-2966.2006.10297.x

Classical novae from the POINT–AGAPE microlensing survey of M31 – II. Rate and statistical characteristics of the nova population

M. J. Darnley,[1]† M. F. Bode,[1] E. Kerins,[1] A. M. Newsam,[1] J. An,[2] P. Baillon,[3] V. Belokurov,[2] S. Calchi Novati,[4] B. J. Carr,[5] M. Crézé,[6,7] N. W. Evans,[2] Y. Giraud-Héraud,[6] A. Gould,[8] P. Hewett,[2] Ph. Jetzer,[4] J. Kaplan,[6] S. Paulin-Henriksson,[6] S. J. Smartt,[2,9] Y. Tsapras[5] and M. Weston[5]

[1]*Astrophysics Research Institute, Liverpool John Moores University, Twelve Quays House, Egerton Wharf, Birkenhead CH41 1LD* [2]*Institute of Astronomy, University of Cambridge, Madingley Road, Cambridge CB3 0HA* [3]*CERN, CH-1211 Genève 23, Switzerland* [4]*Institut für Theoretische Physik, Universität Zürich, Winterthurerstrasse 190, CH-8057 Zürich, Switzerland* [5]*Astronomy Unit, School of Mathematical Sciences, Queen Mary, University of London, Mile End Road, London E1 4NS* [6]*Laboratoire de Physique Corpusculaire et Cosmologie, UMR 7553, CNRS-IN2P3 Collège de France, 11 Place Marcelin Berthelot, F-75231 Paris, France* [7]*Université Bretagne-Sud, Campus de Tohannic, BP 573, F-56017 Vannes Cedex, France* [8]*Department of Astronomy, Ohio State University, 140 West 18th Avenue, Columbus, OH 43210, USA* [9]*Department of Pure & Applied Physics, The Queen's University of Belfast, Belfast BT7 1NN*

Accepted 2006 March 6. Received 2006 February 22; in original form 2005 September 16

ABSTRACT

The POINT–AGAPE (Pixel-lensing Observations with the Isaac Newton Telescope–Andromeda Galaxy Amplified Pixels Experiment) survey is an optical search for gravitational microlensing events towards the Andromeda galaxy (M31). As well as microlensing, the survey is sensitive to many different classes of variable stars and transients. In our first paper of this series, we reported the detection of 20 classical novae (CNe) observed in Sloan r' and i' passbands.

An analysis of the maximum magnitude versus rate of decline (MMRD) relationship in M31 is performed using the resulting POINT–AGAPE CN catalogue. Within the limits of the uncertainties of extinction internal to M31, good fits are produced to the MMRD in two filters. The MMRD calibration is the first to be performed for Sloan r' and i' filters. However, we are unable to verify that novae have the same absolute magnitude 15 d after peak (the t_{15} relationship), nor any similar relationship for either Sloan filter.

The subsequent analysis of the automated pipeline has provided us with the most thorough knowledge of the completeness of a CN survey to date. In addition, the large field of view of the survey has permitted us to probe the outburst rate well into the galactic disc, unlike previous CCD imaging surveys. Using this analysis, we are able to probe the CN distribution of M31 and evaluate the global nova rate. Using models of the galactic surface brightness of M31, we show that the observed CN distribution consists of a separate bulge and disc population. We also show that the M31 bulge CN eruption rate per unit r' flux is more than five times greater than that of the disc.

Through a combination of the completeness, M31 surface brightness model and our M31 CN eruption model, we deduce a global M31 CN rate of 65^{+16}_{-15} yr^{-1}, a value much higher than found by previous surveys. Using the global rate, we derive a M31 bulge rate of 38^{+15}_{-12} yr^{-1} and a disc rate of 27^{+19}_{-15} yr^{-1}. Given our understanding of the completeness and an analysis of other sources of error, we conclude that the true global nova rate of M31 is at least 50 per cent higher than was previously thought and this has consequent implications for the presumed CN rate in the Milky Way. We deduce a Galactic bulge rate of 14^{+6}_{-5} yr^{-1}, a disc rate of 20^{+14}_{-11} yr^{-1} and a global Galactic rate of 34^{+15}_{-12} yr^{-1}, consistent with the Galactic global rate derived elsewhere by independent methods.

Key words: novae, cataclysmic variables – galaxies: individual: M31.

†E-mail: mjd@astro.livjm.ac.uk

© 2006 The Authors. Journal compilation © 2006 RAS

1 INTRODUCTION

Classical novae (CNe) undergo unpredictable outbursts with a total energy that is surpassed only by gamma-ray bursts, supernovae and some luminous blue variables. However, CNe are far more commonplace than these other phenomena (Warner 1989).

Since their first recorded observations, CNe have subsequently been identified as a subclass of cataclysmic variables (CVs). The canonical model for CVs (Crawford & Kraft 1956) is a close binary system, containing a massive C–O or O–Mg–Ne white dwarf (the primary) and a low-mass near-main-sequence late-type dwarf that fills its Roche lobe (the secondary). Any increase in size through evolutionary processes of the secondary results in a flow of material through the inner Lagrangian point into the primary's lobe. The high angular momentum of this transferred material causes it to form an accretion disc around the white dwarf, whilst viscous forces within the disc act to transfer the accreted material inwards, resulting in the accumulation of hydrogen-rich material on the white dwarf's surface (King 1989). In CN systems, the mass accretion rate is generally lower than $10^{-9}\,\mathrm{M}_{\odot}\ \mathrm{yr}^{-1}$ (Cassisi, Iben & Tornambe 1998). As the accreted layer grows, the temperature at the base of the material increases. Hydrogen burning in the accreted envelope soon develops. Given the correct conditions, this can lead to a thermonuclear runaway (TNR) in which the accreted envelope (and possibly some of the 'dredged-up' white dwarf) is expelled from the system in a nova eruption (King 1989; Starrfield & Iliadis, in preparation).

CNe typically exhibit outburst amplitudes of ∼10–20 mag and display an average absolute blue magnitude of $M_{\mathrm{B}} = -8$ at maximum light, with a limit of around $M_{\mathrm{B}} = -9.5$, for the very fastest (Shara 1981b; Warner 1989). The ability to accurately measure the distance to many Galactic novae (using expansion parallax techniques) and a correlation between a nova's luminosity at maximum light and its rate of decline (Hubble 1929; McLaughlin 1945) makes them potentially useful as primary distance indicators. However, until recently, generally poor light-curve coverage, small sample sizes and a current lack of understanding of how the properties of CNe vary between different stellar populations, have severely limited their usefulness as standard candles. Nevertheless, their relatively high frequency allows novae to be used as a tool for mapping the spatial distribution of the population of close binary systems in nearby galaxies. CNe may also be used to test nuclear reaction models and theories, whilst nucleosynthesis during a nova eruption is thought to make a substantial contribution to the abundances of a number of chemical species in the Galaxy such as ^{13}C, ^{15}N and ^{17}O (José 2002).

The 'speed class' of a CN is often used to describe the overall time-scale of an eruption and to classify a nova (McLaughlin 1939; Bertaud 1948). The definition of the various classes depends on the time taken for a nova to diminish by two (or three) magnitudes below maximum light, t_2 (or t_3). Throughout this paper, we will use the speed class definitions given in Warner (1989).

1.1 Maximum magnitude, rate of decline relationship

From his years of observations of CNe in M31, Hubble (1929) noted that the brighter a nova appeared at maximum the more rapidly its visible light diminished. Given that all M31 novae can be considered to lie at equal distance from the observer, Hubble's observation clearly implied a relationship between the nova speed class and its maximum magnitude. These observations for extragalactic novae were later confirmed for Galactic novae by McLaughlin (1945), who used a combination of expansion parallax, interstellar line strengths and Galactic rotation methods to measure the distances of the nearby novae. Over time, the empirically determined maximum magnitude versus rate of decline (MMRD) relationship for CNe has become accepted and refined (Pfau 1976; de Vaucouleurs 1978; Cohen 1985; Downes & Duerbeck 2000).

A recent calibration of the MMRD relationship was made by Downes & Duerbeck (2000) using new distances, derived from expansion parallaxes, for a sample of 28 Galactic novae, and given by

$$M_V = (-11.32 \pm 0.44) + (2.55 \pm 0.32)\ \log\ (t_2/\mathrm{days}). \quad (1)$$

Downes & Duerbeck (2000) concluded that a linear relationship is sufficient to model the Galactic MMRD. They also derived a typical scatter of ∼0.6 mag for CNe about their linear fits. Much of this scatter is thought to be due to difficulties in measuring accurate distances to the novae (Gill & O'Brien 2000; Warner, in preparation; Shafter, in preparation) and from intrinsic scatter in the optical decline due to variations in outburst parameters.

However, it is also known that the linear MMRD relationship is not valid for the fastest and slowest novae (Arp 1956; Schmidt 1957). Novae from M31 and the Large Magellanic Cloud are better described in terms of a 'stretched' S-shaped curve. The form is somewhat supported by theoretical modelling of the nova eruption (Livio 1992). The 'flattening' of the MMRD for brighter novae is thought to be caused as the mass of the white dwarf in the central system approaches the Chandrasekhar limit (Livio 1992). Conversely, the flattening of the MMRD for the fainter novae is thought to be an observational selection effect (Warner 1995).

Capaccioli et al. (1989) were drawn to the conclusion that the same MMRD relationship is valid in all galaxies of all Hubble types. This idea can be exploited to combine data from many different galaxies. As a result, the MMRD relationship can be used as a fundamental distance indicator (Shara 1981a). However, the use of the MMRD relationship as a viable distance indicator is dependent upon being able to measure accurately the maximum brightness of a particular nova and its speed class, requiring good sampling of both the maximum light and the decline.

1.2 Absolute magnitude 15 d after peak

Buscombe & de Vaucouleurs (1955) observed that all CNe appeared to reach approximately the same absolute magnitude 15 d after their maximum light (M_{15}). The apparent constancy and value of M_{15} is yet to be fully explained, despite attempts to place it on a more physical footing (Shara 1981b). Sometimes referred to as the t_{15} relationship, a recent calibration was carried out by Ferrarese, Côté & Jordán (2003) using nine newly discovered novae from *Hubble Space Telescope* (*HST*) observations of M49. Their calibration is

$$M_{15,V} = -6.36 \pm 0.19\ (\mathrm{random}) \pm 0.10\ (\mathrm{systematic}). \quad (2)$$

However, there is great inconsistency in the calculated values of M_{15} (see table 2.4 of Warner, in preparation). More recent results have called into question the reliability of using this so-called t_{15} relationship for distance derivations and the validity of the relationship itself (Jacoby et al. 1992; Ferrarese et al. 2003).

Table 1. r' and i' maximum observed magnitudes and corresponding t_2 times, maximum magnitude uncertainties and average extinction correction (in magnitudes) for each CN detected in the POINT–AGAPE data.

Nova	$r'(t_0^{r'})$	$t_2(r')$	Estimated max error on r' maximum light	Estimated average r' extinction	$i'(t_0^{i'})$	$t_2(i')$	Estimated max error on i' maximum light	Estimated average i' extinction
PACN-99-01	16.53 ± 0.03^a	30.50	–	−0.67	16.39 ± 0.03^a	37.53	–	−0.51
PACN-99-02	18.91 ± 0.03	99.48	−0.03	−0.57	19.19 ± 0.04	58.09^d	−0.04	−0.43
PACN-99-03	17.79 ± 0.02	59.62	−0.02	−0.60	17.60 ± 0.04	34.16	−0.06	−0.46
PACN-99-04	18.41 ± 0.04	164.39^d	−0.02	−0.52	18.34 ± 0.07	87.25^d	−0.02	−0.39
PACN-99-05	17.70 ± 0.04	25.82	−0.04	−0.66	–	–	–	−0.50
PACN-99-06	16.17 ± 0.01	20.30	−0.13	−0.67	–	–	–	−0.51
PACN-99-07	18.1 ± 0.1	9.80	−4.2	−0.65	18.02 ± 0.04	2.28	−0.88	−0.49
PACN-00-01	17.73 ± 0.04^b	38.65	–	−0.58	17.58 ± 0.08^b	11.88^d	–	−0.44
PACN-00-02	18.15 ± 0.03	198.55	−0.01	−0.65	18.85 ± 0.05	817.19^d	-0.00^a	−0.49
PACN-00-03	18.54 ± 0.03	33.02	−0.06	−0.67	18.19 ± 0.04	22.44^d	−0.09	−0.51
PACN-00-04	17.61 ± 0.03	30.65	−0.07	−0.66	17.33 ± 0.04	36.44^d	−0.06	−0.50
PACN-00-05	17.30 ± 0.01	59.21	−0.18	−0.65	17.11 ± 0.01	198.32	−0.06	−0.49
PACN-00-06	17.09 ± 0.01	13.85	−0.09	−0.65	16.64 ± 0.01	13.44	−0.14	−0.49
PACN-00-07	19.53 ± 0.04	55.21	−0.03	−0.48	19.48 ± 0.05	100.27^d	−0.02	−0.37
PACN-01-01	18.45 ± 0.02^c	213.12^d	–	−0.61	18.16 ± 0.04^c	330.86^d	–	−0.47
PACN-01-02	17.14 ± 0.03	22.06	−0.10	−0.64	16.71 ± 0.04	17.08	−0.12	−0.48
PACN-01-03	17.30 ± 0.04	143.71	−0.02	−0.62	16.88 ± 0.06	66.21^d	−0.03	−0.47
PACN-01-04	17.90 ± 0.03	47.29	−0.05	−0.65	17.38 ± 0.04	37.24	−0.06	−0.49
PACN-01-05	15.90 ± 0.01	28.15	−0.93	−0.57	15.61 ± 0.01	15.83	−1.68	−0.43
PACN-01-06	17.38 ± 0.01	52.13	−0.12	−0.63	16.88 ± 0.03	38.24^d	−0.10	−0.48

[a]The light-curve of PACN-99-01 was visible at, or shortly after, maximum light in the first observational epoch of the first season, so it was only possible to put a lower limit on its maximum light; [b]as PACN-99-01 for the second season; [c]as PACN-99-01 for the third season; [d]it was not possible to follow these light-curves through two magnitudes below their observed maxima, so the value of t_2 has been estimated from the general trend of these light-curves.

1.3 CN in M31 and the global nova rate

A large number of CN surveys in M31 have been carried out, resulting in the discovery of around 500 novae. These have indicated the global nova rate in M31 to be $\sim$30–40 yr^{-1} (Shafter & Irby 2001). Table 1 in Darnley et al. (2004, hereafter Paper 1) summarizes the findings of many of these past surveys. The relatively high nova rate in M31 and its close proximity to our own Galaxy are major advantages of targeting M31 for nova surveys. However, since M31 is nearer edge-on than face-on, with an inclination angle of $\sim$77° (de Vaucouleurs 1958), the task of unambiguously distinguishing between novae erupting within the disc or within the bulge is rather difficult (Hatano et al. 1997). Consequently, there remains a debate surrounding the distribution and rate of novae within M31. The large inclination angle also introduces additional extinction complications.

The early M31 CNe surveys of Arp (1956) and Rosino (1964) found that the nova distribution decreased significantly towards the centre of the bulge, with Rosino (1973) reporting the centre of the bulge to be '*devoid of novae*'; all of this was despite their attempts to detect novae within the central bulge regions. Such studies were hampered by saturation effects when using photographic plates as opposed to CCD detectors. However, the first M31 Hα survey (Ciardullo et al. 1987) found that the nova distribution follows the galactic light all the way into the centre of the bulge. A combination of the Arp (1956) novae with the Ciardullo et al. (1987) catalogue yielded the result that the bulge nova rate per unit B light was an order of magnitude greater than that of the disc, implying that the vast majority of the M31 novae arise from the bulge population. This result was later confirmed by Capaccioli et al. (1989) after undertaking a comprehensive analysis of all M31 CN data. However, there is the potential for biases due to extinction, especially within the disc, as the Hα surveys had focused primarily on the bulge, using much earlier B-band surveys to 'fill in' the disc data. In an attempt to tackle the lingering extinction issues, Shafter & Irby (2001) extended the Hα observations further into the M31 disc. Using M31's planetary nebula distribution for comparison, they arrived at the conclusion that the M31 CN distribution is consistent with an association with the bulge.

1.4 Nova populations

The idea that CNe may arise from two distinct populations was first postulated by Duerbeck (1990). This was further explored by della Valle et al. (1992) who presented evidence that fast novae were concentrated closer to the Galactic plane than slower novae. Additional spectroscopic data have revealed that there may exist two spectroscopic classes of CNe, the Fe II and He/N novae (Williams 1992). It has been shown that the He/N novae tend to cluster close to the Galactic plane and that they tend to be brighter and faster than the Fe II type (della Valle & Livio 1998).

Theoretical studies of CN outbursts (e.g. Shara, Prialnik & Shaviv 1980; Shara 1981a; Prialnik et al. 1982; Livio 1992; Prialnik & Kovetz 1995) have shown that the form of the outburst depends upon properties such as the white dwarf's mass, accretion rate and luminosity. These white dwarf properties may vary with the underlying stellar population. These findings lend support to the idea that CNe in differing stellar populations may have distinctly different outburst properties.

The surface gravity of a white dwarf increases with increasing white dwarf mass. This leads to a higher pressure at the base of the accreted envelope when the TNR begins, resulting in a more powerful outburst. It also follows that, as the pressure at the envelope base is greater for more massive white dwarfs, a lower mass of accreted material is required for the envelope to achieve the temperature and density required for a TNR to be initiated. Thus, the more massive white dwarfs are expected to have shorter recurrence times and to exhibit faster light-curve evolution.

1.5 The POINT–AGAPE CNe catalogue

In Paper 1, we presented an automated pipeline that used objective selection criteria to detect and classify CNe within a data set with good temporal sampling. We reported 20 CNe erupting within M31 over three seasons, detected using the pipeline. Nine of these CNe were caught during the final rise phase and all were well sampled in at least two colours. The excellent light-curve coverage allowed us to detect and classify CNe over almost the full range of speed classes.

For the purposes of the POINT–AGAPE (Pixel-lensing Observations with the Isaac Newton Telescope–Andromeda Galaxy Amplified Pixels Experiment) microlensing survey, the Wide Field Camera (WFC) on the Isaac Newton Telescope (INT), situated at La Palma, was used to regularly monitor two M31 fields between 1999 August and 2002 January. The field centres were located at $\alpha = 0^{\rm h}44^{\rm m}00\overset{\rm s}{.}0$, $\delta = +41^{\circ}34'00\overset{''}{.}0$ and $\alpha = 0^{\rm h}43^{\rm m}23\overset{\rm s}{.}0$, $\delta = +40^{\circ}58'15\overset{''}{.}0$(J2000) The WFC consists of a mosaic of four 2048×4100 pixel CCDs and the field locations are indicated in fig. 1 in Paper 1. The field placements were primarily chosen to be sensitive to compact dark matter candidates, or massive compact halo objects, which are predicted to be most evident towards the far side of the M31 disc (Kerins et al. 2001). The observations were conducted over three seasons in at least two broad-band Sloan-like passbands (usually r' and i', augmented with g' during the first season). The full distribution of observations can be seen in table 3 and fig. 2 in Paper 1.

The outline of the current paper is as follows. In Section 2, we discuss our treatment of the internal extinction of M31. Section 3 presents our analysis of the MMRD relationship for M31. The t_{15} analysis is presented in Section 4. In Section 5, we describe in detail our completeness analysis of the POINT–AGAPE data set and the CN detection pipeline. In Section 6, we present our analysis of the CN population of M31. Section 7 details our evaluation of the global CN rate of M31, and finally we summarize and discuss our main findings in Section 8.

2 EXTINCTION ESTIMATION

In M31, as with most disc and spiral galaxies, the vast majority of the dust lies close to the disc plane and the extinction is patchy (Holwerda et al. 2005). As such, we expect that novae within M31 should suffer a varying range of extinction, dependent upon their position in the plane of the galaxy and their line-of-sight displacement. These extinction uncertainties may be problematic when trying to analyse some of the global properties of the POINT–AGAPE CN catalogue, such as the MMRD and t_{15} relationships, as well as the completeness, CN population and nova rate.

To compute the extinction across different parts of the M31 disc we employ synthetic stellar models (Girardi & Salaris, 2001, Salaris, private communication) to estimate the extinction-free integrated colour ($\langle r' - i' \rangle$) of the disc, assuming a mean underlying colour which is constant with radius. This is compared to the observed $\langle r' - i' \rangle$ colour map of M31 (An et al. 2004, see their fig. 2) to allow us to compute an extinction map. Assuming that the M31 reddening curve is similar to that in the Milky Way, the theoretical and observed colours yield an extinction map for each band. The extinction model does show a decrease towards larger disc radii, as one would expect, and the highest extinction regions correspond to the prominent dust lanes which are evident on the north-western side of M31.

The global average for the extinction maps are all rescaled to give a global average extinction though the disc of $A(i) = 0.8$, corresponding to the typical value for Sb galaxies found by (Holwerda et al. 2005, see their fig. 11) after transforming to Sloan magnitudes (Schlegel, Finkbeiner & Davis 1998). Without this rescaling, our extinction values are systematically high, which we suspect may be because our synthetic models contain a larger fraction of bluer stars than is typically present in the M31 disc. We also note that the foreground Galactic extinction of $A(i) = 0.13$ is assumed constant across M31 (Darnley 2005; Holwerda et al. 2005).

3 THE MMRD RELATIONSHIP

As noted earlier, the MMRD relationship is important as it can potentially be used as a tool to derive the distance to an extragalactic population of CNe by comparison to the MMRD in our own Galaxy.

The CN decline rates originally estimated for the 20 detected POINT–AGAPE novae (see table 6 of Paper 1) are recomputed for this analysis. To calculate the value of t_2 for each CN, we linearly interpolate between points on the decline of each light-curve. This is carried out for both the r' and i' observations. The g' observations are omitted as they are only available for seven of the detected novae.

The measured maximum light and computed t_2 values for each CN candidate are shown in Table 1. The novae PACN-99-01, PACN-00-01 and PACN-01-01 are excluded because they are likely already to have been in decline at first observation; hence it is not possible to accurately determine the uncertainty in their maximum light or decline rate. In addition, only a small portion of the light-curve of PACN-99-07 is sampled. As such, due to its erratic behaviour, we are doubtful whether the classification as a very fast nova is a true representation of this nova's speed class. Also, there are no i' data available around maximum light for PACN-99-05 and PACN-99-06, so it is not possible to determine a t_2 value for these novae. Therefore, only 16 novae are used for the r' MMRD analysis and 14 novae for the i' analysis.

An initial evaluation of the linear MMRD relationship for both the r' and i' data produces a poor fit, in the sense that the scatter of both distributions is much greater than that implied solely by the photometric uncertainties.

3.1 Maximum light uncertainties

In an attempt to refine further our MMRD relationship, and either reduce or help to explain the large scatter, we allow that the brightest observation of each nova is only a lower limit to that nova's true maximum light. In the majority of cases each maximum observation is straddled by observations from the following and preceding nights, leading to a small error in the assignment of the true maximum light. We then estimate the maximum potential error on our measurement of the maximum light. Taking a good estimation

of the general slope of each light-curve to be $2/t_2$ mag d^{-1}, we calculate the amount that each light-curve could have possibly increased in brightness between the two points straddling the brightest observation. The maximum potential error induced by missing the maximum light for each CN is also shown in Table 1. The large maximum light errors derived for PACN-99-07 and PACN-01-05 are due to a combination of a fast decline rate and poor sampling around maximum light. In particular, the speed class assignment of PACN-99-07 is known to be suspect; a much slower decline time seems more fitting. As previously mentioned, this CN is excluded from this analysis due to the uncertainty of its decline rate.

The photometric and maximum light uncertainties are combined by simple addition as the maximum light error is a systematic rather than a random error. The actual maximum light is equally likely to lie at any point between the observed value and the computed potential maximum value. For the purpose of fitting the MMRD relationship, we 'resample' the 'observation' of the maximum light to be the midpoint of the computed range for each CN.

We use a minimum absolute deviation method to fit the data, as our errors are no longer Gaussian and are dominated by uniformly distributed systematic uncertainties. The scatter on these MMRD fits remains at ∼0.6 and ∼0.7 mag for the r' and i' data, respectively. This implies that the scatter in the MMRD relationships is not significantly affected by missing the maximum by a day or two, as is the typical interval expected in the POINT–AGAPE data. The similarity between these fits and those performed without considering the maximum light uncertainties is also indicative of the apparent minimal effect induced by considering the possibility of missing the maximum light of a CN.

3.2 Extinction corrections

Each CN's light-curve may still be affected by extinction within M31 and our own Galaxy. The Galactic extinction in the direction of M31 is well defined and relatively small compared to the maximum potential extinction experienced within M31. The extinction experienced by each nova's light depends upon the column density between the nova and the observer, with the maximum potential extinction dependent upon the CN's position.

We use the extinction maps (see Section 2) to provide an estimate of the maximum potential extinction experienced by each of the 16 CNe for which valid r' decline rates could be computed and by each of the 14 novae with valid i' decline rates. The computed average extinctions are shown in Table 1. Fig. 1 shows the distribution of extinction corrected and maximum magnitude corrected r' and i' data, respectively. The base of the error bars represents the true maximum observed light, with the length of the bars representing the absolute range of the actual maximum light. As with the maximum magnitude errors, we assume that the extinction is equally likely to lie at any value between zero and the maximum estimate. Again, for this analysis, the three error sources are combined by simple addition. As the maximum light error and the extinction error are both independent absolute maximum errors, the maximum error that can be experienced due to both of these sources is simply the sum of the two – in the direction of increasing luminosity. We again assume that the best guess maximum light flux occurs equally distant between the observation and the extreme maximum error for the purpose of the MMRD fitting. The fits to the maximum light estimates are

$$m_{r'} = (14.5 \pm 1.3) + (1.5 \pm 0.8) \log (t_2/\text{days}), \quad (3)$$

$$m_{i'} = (14.5 \pm 1.0) + (1.5 \pm 0.6) \log (t_2/\text{days}). \quad (4)$$

The scatter in the final MMRD fits is ∼0.7 and ∼0.8 mag for the r' and i' data sets, respectively, comparable to the mean error size. The MMRD data are also analysed in the linear region of the 'S-shaped' curve ($0.5 \leqslant \log [200d/t_2] \leqslant 1.5$), yielding

$$m_{r'} = (13.0 \pm 2.2) + (2.5 \pm 1.4) \log (t_2/\text{days}), \quad (5)$$

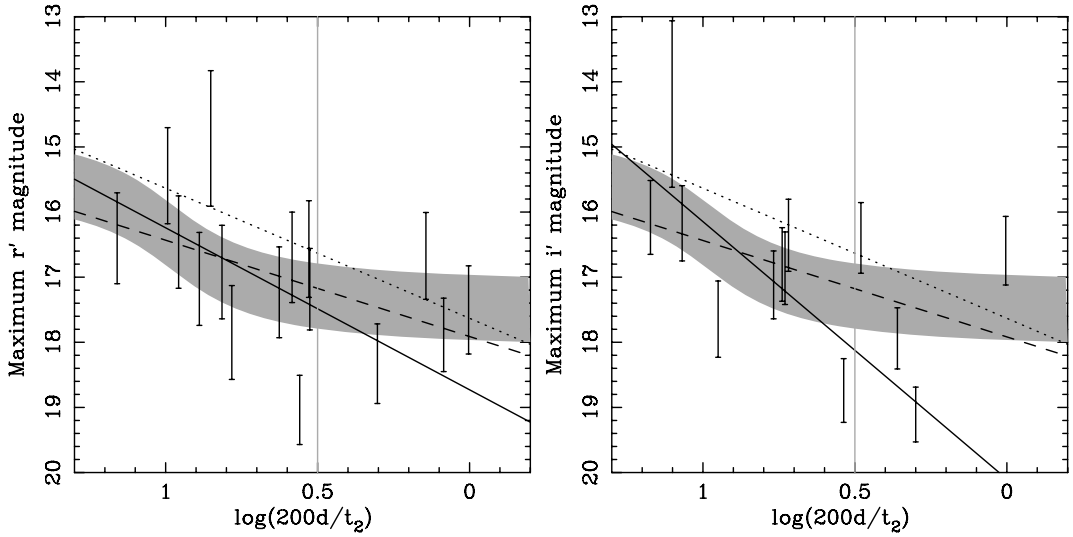

Figure 1. The relationship between the r' brightness at maximum light and the decay rate $\{v_2(r') = \log [200d/t_2(r')]\}$ of the 16 POINT–AGAPE CNe with well-defined maximum lights and decay rates (left-hand panel). Likewise for i' maximum light (right-hand panel). The range of the error bars represents the maximum estimated range of the combination of the extinction, maximum light and observational uncertainties. The dashed line indicates an unweighted fit performed on all the data (equation 3), while the solid line shows an unweighted fit performed on the data in the range $0.5 \leqslant \log [200d/t_2(r')] \leqslant 1.5$ (see equation 5). The vertical grey line represents the 'slow' boundary of the linear region of the MMRD $\{\log [200d/t_2(r')] = 0.5\}$. The grey shaded region represents the best-fitting Galactic 'S-shaped' MMRD, and the black dotted line shows the best-fitting Galactic linear MMRD - both these Galactic MMRD relationships are derived for V data and have been transformed to the M31 distance.

© 2006 The Authors. Journal compilation © 2006 RAS, MNRAS **369,** 257–271

$$m_{i'} = (11.0 \pm 2.4) + (3.9 \pm 1.6) \log (t_2/\text{days}), \quad (6)$$

with a scatter of ∼0.7 mag about the fits for both the r' and i' data, which is again comparable to the mean error.

All four of the MMRD relationships calculated (equations 3–6) are shown in Fig. 1, along with a recent Galactic calibration of the MMRD relationship (equation 1 in Downes & Duerbeck 2000). The Downes & Duerbeck (2000) calibration has been translated to the distance of M31 using a distance modulus of 24.3 mag (Welch et al. 1986), yielding

$$m_V = (12.98 \pm 0.44) + (2.55 \pm 0.32) \log (t_2\ /\text{days}). \quad (7)$$

It is clear that neither the r' nor i' MMRD relationships provide enough data points to investigate in greater detail the true form (linear of S-shaped) of the M31 MMRD relationship. As previous work (see Section 1.1) has specifically identified a linear region within M31's MMRD relationship, we will use the relationships defined within the linear region (shown in equations 5 and 6) as the r' and i' MMRDs for M31.

We note that extinction is a rather weak factor in determining the slope of the MMRD in the linear regime, where all the novae are intrinsically very bright [$M(r') < 18$]. Indeed, our MMRD slope determination with or without the extinction correction is essentially the same.

4 THE T_{15} RELATIONSHIP

As discussed earlier, the t_{15} relationship may also be useful in calculating the distance to a CN population. The majority of previous t_{15} calibrations have been carried out using V-band data. However, due to the restrictions of the POINT–AGAPE catalogue, we can only attempt calibration using r' and i' data.

Using these data, an initial calibration of the t_{15} relationship for the POINT–AGAPE catalogue indicates that the photometric errors alone do not account for the extent of the scatter of luminosities at 15 d following maximum light.

As was attempted for the MMRD data, we can try to decrease or at least explain the scatter in these data by taking into account the line-of-sight extinction. Using the data in Table 1 to recalibrate each light-curve, we therefore reassess both the r' and $i't_{15}$ relationships for the POINT–AGAPE novae catalogue:

$$m_{15,r'} = 18.0 \pm 0.9, \quad (8)$$

$$m_{15,i'} = 18.0 \pm 1.0. \quad (9)$$

Fig. 2 shows superpositions of the 16 r' and 14 i' recalibrated light-curves that have well-defined maximum light magnitudes. The light-curves are all plotted in units of time since maximum light. Each plot shows the light-curve behaviour for the first 50 d following each eruption. There is clearly little or no convergence of these light-curves at a time of around 15 d.

The inclusion of extinction and maximum light uncertainties has actually slightly increased the scatter of the t_{15} values. This implies that the scatter in luminosities 15 d after peak is not solely due to uncertainties in the luminosity of the nova, indicating that any t_{15} relationship may not be valid for these passbands.

4.1 Comparison with previous results

By assuming a distance modulus for M31 of 24.3 mag (Welch et al. 1986), our computed t_{15} values (see equations 8 and 9) are given by

$$M_{15,r'} = -6.3 \pm 0.9, \quad (10)$$

$$M_{15,i'} = -6.3 \pm 1.0. \quad (11)$$

However, direct comparison between our results and previous results cannot easily be made. All calibrations of the t_{15} relationship to date have been in 'blue' bands, whereas our calibration is performed in 'red' bands. Nevertheless, given that CNe are expected to become

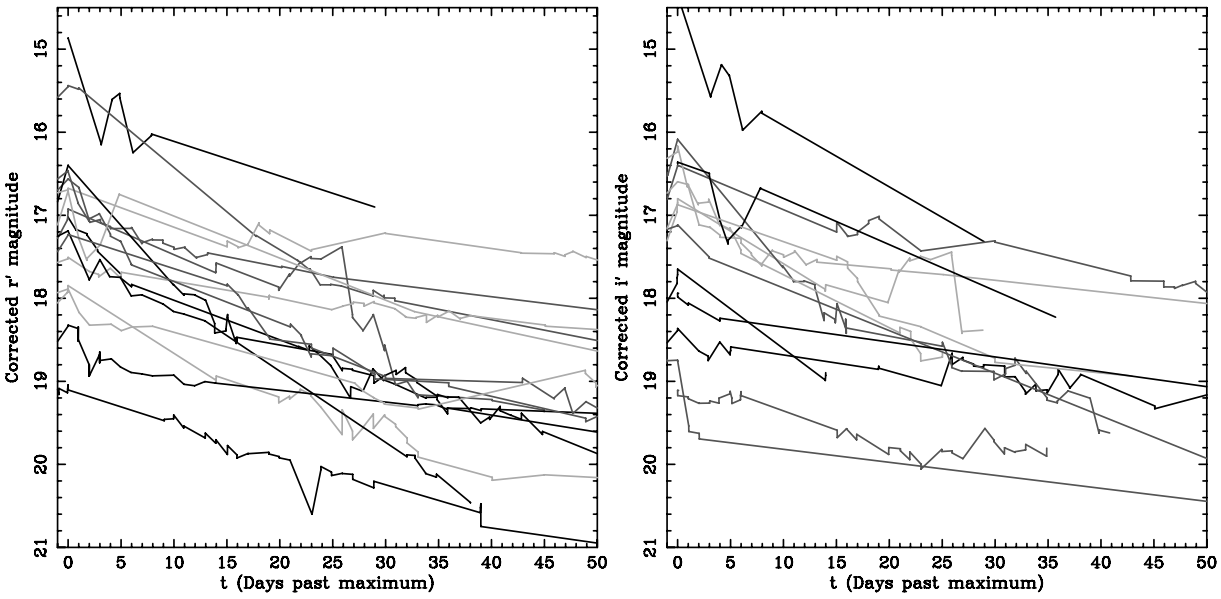

Figure 2. A superposition of the recalibrated r' light-curves of 16 of the POINT–AGAPE CNe (left-hand panel) and the superposition of the recalibrated i' light-curves of 14 of the POINT–AGAPE CNe (right-hand panel). The light-curves have been time shifted so that the times of their observed maximum light are coincident. Each line represents the linear interpolation of the light-curves between observations.

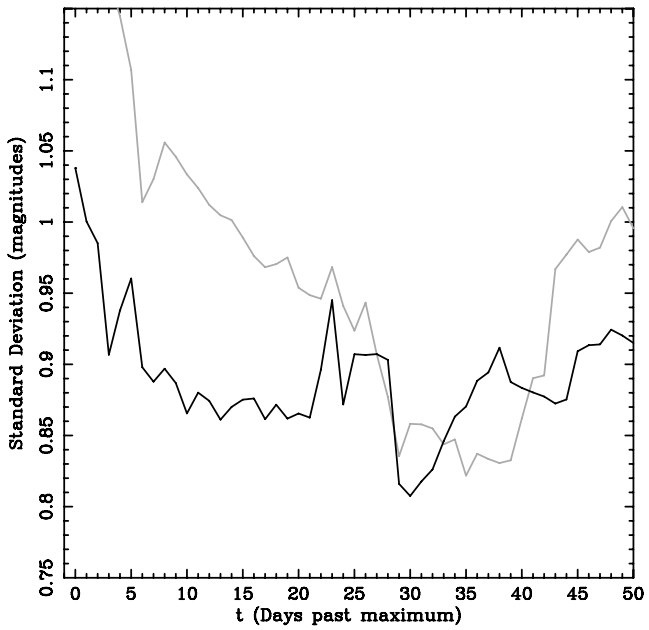

Figure 3. Plot of the distribution of r' magnitude scatter (black line) and the i' magnitude scatter (grey line) between observed nova magnitudes for a range of times following maximum light.

bluer with time, the result that our t_{15} luminosities are fainter than all but the most recent of the previous 'blue' calibrations (see table 2.4 of Warner, in preparation) is not surprising. The scatter in our results is very large, and larger than those found in previous surveys. For instance, in a recent *HST* study of M49 (Ferrarese et al. 2003) the V-band t_{15} relationship was found to have $\sigma = 0.43$ mag. It should also be noted that, as an elliptical galaxy, M49 does not suffer from problems due to large internal extinction. However, the large degree of the scatter in the POINT–AGAPE data cannot be solely explained by the combination of maximum light and extinction uncertainties, whose mean error is $\sim$0.7 mag for both the r' and i' data.

As a final test, if the t_{15} relation is valid, then we would expect a minimum in the scatter of the light-curves at or around 15 d after maximum light. Fig. 3 shows a plot of the scatter between the POINT–AGAPE light-curves over a large range of time following maximum light for the r' and i' data. From inspection of this plot, it is quite clear that the light-curves of the POINT–AGAPE sample do not exhibit behaviour consistent with the existence of a t_{15} relationship. However, the r' scatter does seem to exhibit a minimum at $\sim$30 d after maximum light and the i' scatter is minimized $\sim$35 d following maximum. However, these minima are coincident with the end of data sampling for a number of the light-curves, so may just be indicative of the temporal coverage of the POINT–AGAPE light-curves themselves.

5 CN DETECTION PIPELINE COMPLETENESS

Because we have selected our nova candidates using objective selection criteria, we can assess the efficiency of our selection pipeline. This allows us to compute the completeness of the POINT–AGAPE CN catalogue and aids us in probing the underlying CN distribution and to compute a robust estimate of the actual underlying global nova rate. To measure the completeness of the catalogue, we seed the raw POINT–AGAPE data with resampled light-curves of our 20 detected CNe. We then rerun the entire CN detection pipeline on these seeded data to allow us to compute the proportion of recovered light-curves.

5.1 Creating test light-curves

The seeded light-curves are positioned on a grid within the aligned image data stack (see Section 3 in Paper 1), with a grid spacing of 15 pixels (5 arcmin). This grid spacing is chosen to allow the closest possible spacing of seeded objects, whilst minimizing overlap of each star's point spread function (PSF). Each light-curve is seeded at a random eruption epoch, such that at least one point of the light-curve occurred between the first observational epoch and the final epoch.

In order to seed the detected novae at any random time, we linearly interpolate their light-curves between successive observations. Whilst this works well when the time-scale between observations is small, it becomes less reliable when the gaps are larger. The largest gaps in the observations are usually of order 2 weeks, but in a few cases, when light-curves are followed across two seasons, these are up to six months. The two light-curves affected by this are PACN-00-02 and PACN-00-05 (see Section 5 of Paper 1), these light-curves being linearly interpolated across the seasonal gaps. Given the form of the light-curve of PACN-00-02, we expect this method to be relatively reliable as an estimate of the flux. However, given the predicted transition phase minimum for PACN-00-05, this estimate is much less reliable.

5.2 Seeding the raw POINT–AGAPE data

The generated light-curves are added to both the raw data and the PSF-matched data (see Section 3.2 of Paper 1) using the National Optical Astronomy Observatories (NOAO) IRAF package environment[1] MKOBJECTS, which scales the relevant image's PSF profile to the correct luminosity, then adds the scaled PSF profile to the data, recalculates the Poisson errors and combines these with the data.

5.3 Rerunning the nova detection pipeline

The CN detection pipeline is rerun on the seeded data; however, a number of stages of the pipeline are not used. As both the raw and the PSF-matched data are seeded independently,[2] the image alignment, trimming, PSF-matching and background estimate stages are not required.

The seeded PSF-matched data are run though the aperture photometry pipeline (see Sections 4.2 and 4.3 of Paper 1) to produce the preliminary list of recovered light-curves. PSF-fitting photometry is then performed at the position of each of the seeded novae recovered from the aperture photometry stage. These nova light-curves are then passed back through the 'peak detection' stage of the pipeline. However, all of the pipeline stages that are related to the colour light-curves are ignored. We are able to ignore the colour criteria as these are solely introduced to distinguish CN light-curves from the light-curves of other objects that may have passed through

[1] IRAF is distributed by the National Optical Astronomy Observatories, which are operated by the Association of Universities for Research in Astronomy, Inc. under cooperative agreement with the National Science Foundation.
[2] In order to maintain consistency between the seedings in the raw and PSF-matched data, the same random seed is used to regenerate the Poisson noise for both CN seedings.

Table 2. The effect of each stage of our selection pipeline upon the synthetic CN catalogue. These steps are described in Section 4 of Paper 1.

Pipeline stage	North field				South field				All
	CCD1	CCD2	CCD3	CCD4	CCD1	CCD2	CCD3	CCD4	CCDs
Seeded objects	35 239	35 376	35 244	35 376	35 910	35 239	35 378	34 864	282 626
Objects seeded within data	18 291	18 886	18 314	18 401	14 185	18 082	18 861	18 527	143 547
10σ objects	16 519	17 569	17 339	17 107	13 352	16 216	17 667	17 049	132 818
Pipeline 1st pass – aperture photometry									
Five consecutive detections	13 457	14 982	14 945	14 428	12 451	14 573	15 849	15 303	115 988
$\geqslant$1 primary peak	13 078	14 768	14 660	14 106	12 221	14 196	15 409	14 789	113 227
Periodicity test	12 979	14 676	14 550	13 965	12 156	14 118	15 191	14 583	112 218
Primary peak height	12 859	14 564	14 477	13 784	12 113	13 945	14 938	14 391	111 071
Secondary peak height	11 011	11 642	12 460	11 253	10 373	11 926	11 062	11 179	90 906
Pipeline 2nd pass – PSF-fitting photometry									
Five consecutive detections	9 981	11 549	12 330	11 191	10 157	11 502	10 628	10 787	88 125
$\geqslant$1 primary peak	9083	11 056	11 907	10 696	9728	10 837	9978	10 157	83 442
Periodicity test	9083	11 056	11 907	10 696	9728	10 837	9978	10 157	83 442
Primary peak height	8868	10 805	11 531	10 420	9461	10 591	9805	9909	81 390
Secondary peak height	8169	10 433	10 994	9 938	9290	10 209	9619	9682	78 334
Further candidate elimination stages									
$<$90 per cent of points in peaks	8141	10 403	10 968	9 911	9 274	10 185	9605	9 654	78 141
Five g' or i' points	–	–	–	–	–	–	–	–	–
Colour evolution	–	–	–	–	–	–	–	–	–
Rate of decline	–	–	–	–	–	–	–	–	–
Colour–magnitude criteria	–	–	–	–	–	–	–	–	–
Final candidates	8 141	10 403	10 968	9938	9274	10 185	9605	9 654	78 141

the previous stages of the pipeline.[3] However, as we know that all 20 of the seeded light-curves are those of CN discovered in the POINT–AGAPE data, they have already passed the colour criteria.

A seeded CN light-curve may 'fail' the pipeline for any of the following reasons.

(i) The object has been seeded at a location in the M31 field where, due to the brightness of the background and/or surrounding objects, it is impossible to make a 10σ detection of the object at any epoch.

(ii) There are not five consecutive detections, either because the object is too faint to detect or because it has been seeded such that there are not five observations in which the nova was visible.

(iii) The observed 'peak' of the seeded nova is not significant enough to pass the primary peak test. This is either due to the galactic background or because the nova has been seeded 'low down' in its light-curve, i.e. the actual peak has not been seeded in any of the observations.

(iv) A seeded CN light-curve can fail the periodicity test, the secondary peak height test or the '$<$90 per cent of points in peaks' test, if the nova has been seeded close to a region of the image that also varies significantly with time. This may be due to a nearby variable star, a region of bad pixels or a saturated object. Again, it is possible for a light-curve to fail this test if data around the actual peak of the nova have not been seeded.

The numerical results of the completeness run of the CN pipeline are shown in Table 2.

[3]The make-up of the POINT–AGAPE observation strategy makes it impossible to seed i'- and g'-band data across observing seasons as there is minimal i'-band data available for the first season and no g'-band data available for the second or third.

5.4 Completeness distribution

In order to compute the completeness, we subdivide each CCD into 1-arcmin grid squares, with each grid square containing 144 novae seed points. Depending upon the size of the trimmed CCDs (see Section 3.1 of Paper 1), the CCDs contain between 200 and 242 grid squares.

We first compute the completeness distribution of the CN pipeline; this distribution tells us the probability of the pipeline detecting a CN – of a type originally detected by the pipeline – at any position in the POINT–AGAPE fields, given that the CN in question is 'visible' at least once between (and including) the first and last observations. This completeness calculation takes account of all of the major factors that affect the completeness of the detection pipeline, including the temporal distribution of the POINT–AGAPE observations, the galactic surface brightness, the variety of CN light-curve forms and any interference by foreground objects.

The generated completeness map is shown in Fig. 4. This illustrates that the completeness is relatively flat across both fields, within the noise, at a value between about 30–40 per cent. However, the completeness does decline towards the centre of the galaxy, as the galactic background begins to increase significantly.

6 M31 CN POPULATION

If we adopt the simplest assumption that the nova distribution in M31 follows the light distribution (Ciardullo et al. 1987), then the probability of a CN erupting at a particular point within M31 is proportional to the flux at that position. By requiring that a given CN erupts within one of the two POINT–AGAPE fields, we can compute the probability of a CN erupting at a particular point within M31. However, from our completeness calculations, we also know the probability of detecting a CN in each grid square, given that a nova erupts within that square. Hence, we can use this to calculate the probability of detecting a CN within the POINT–AGAPE fields,

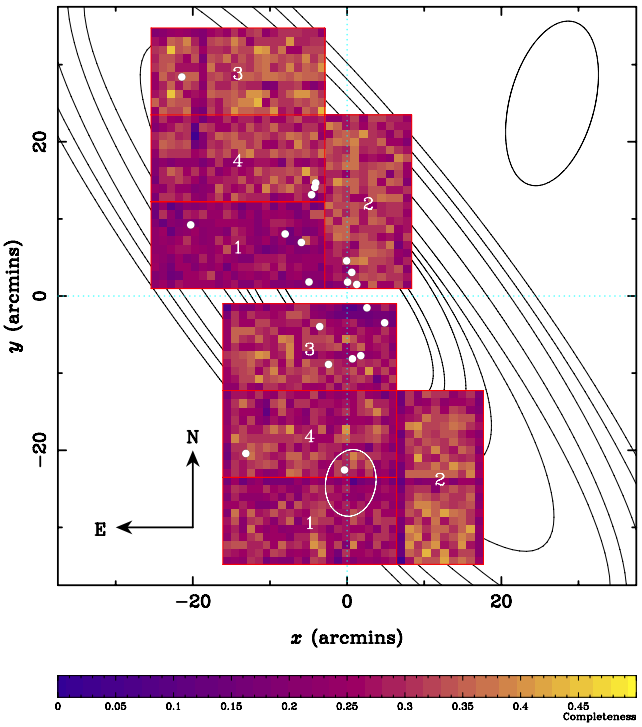

Figure 4. The POINT–AGAPE CNe detection pipeline completeness distribution. Each numbered region represents one of the four INT WFC CCDs and the white circles indicate the positions of the 20 detected novae. The origin is the centre of M31 at (J2000)$\alpha = 0^{\rm h}42^{\rm m}44\overset{\rm s}{.}324$, $\delta = +41^\circ16'08\overset{''}{.}53$ (Crane, Dickel & Cowan 1992). Also, indicated are 10 representative M31 'isophotes' from the surface photometry of de Vaucouleurs (1958), along with representations of the positions and sizes of M32 (within the southern field) and NGC 205.

given that a nova erupts within them. This detection probability is given by

$$P_i = \frac{f_i}{\sum_{j=1}^{N_{\rm bins}} f_j}\varepsilon_i, \tag{12}$$

where P_i is the probability of a CN erupting in a particular grid square containing a flux f_i and ε_i is the computed pipeline efficiency in the grid square in question. Because of the uniformity of ε, the distribution of detection probabilities closely resembles the galactic light. However, as the completeness drops slightly towards the galactic centre, this distribution has a slightly weaker central dependence than the flux.

If M31 consisted solely of a single population of stars, then the 'nova follows the light' distribution would be a good model of the CN distribution. However, with recent evidence pointing towards separate bulge and disc populations of novae (see Section 1.4), it is likely that the detection probability model (equation 12) needs to be modified.

6.1 Modelling M31's galactic light

In order to calculate the overall CN rate of M31 or to investigate the possibility of separate bulge and disc CN populations, we need to be able to compute both the bulge and disc component of the light at any given point within the galaxy. In order to do this, we need to create a model of the flux distribution of M31. To perform this modelling, we subdivide each CCD using the 1-arcmin square grid system that we employed for the completeness calculations.

In order to try to fit the disc or bulge components of the M31 light, we first define a region of the galaxy within which either the bulge or the disc light could be unambiguously defined. In the outer regions of a spiral galaxy such as M31, the visible light arises almost completely from the disc. Therefore, it is possible to model the disc in these regions and extend the model to the inner regions of the galaxy.

To greatly simplify the geometry of the galactic disc, we make the assumption that it is thin with an inclination of 77° (de Vaucouleurs 1958) and that the flux distribution is smooth across the disc. Another simplification we make is to essentially collapse the disc into a one-dimensional system. Each position within the disc is transformed to the semimajor axis of the ellipse that passed through that point. As the light from a galactic disc can often be modelled using a simple exponential law (Freeman 1970), the disc flux at any point within M31 can then be defined as

$$f_{\rm d}(a_{\rm d}) = f_{\rm d}^0\ {\rm e}^{-a_{\rm d}/a_{\rm d}^0}, \tag{13}$$

where $f_{\rm d}(a_{\rm d})$ is the disc flux at a position within the disc with semimajor axis $a_{\rm d}$. As it is not possible to unambiguously separate disc light from bulge light, the fit is performed to the total flux data for $a_{\rm d} \geqslant 40$ arcmin in order to have minimal contamination from the bulge light. The best-fitting values found for the two parameters are, $f_{\rm d}^0 = 3676$ adu pixel^{-1} and $a_{\rm d}^0 = 43.1$ arcmin.

In order to attempt to fit the bulge flux, we extend the disc model across the whole galaxy and then subtract the modelled disc light from the galactic light to leave just the bulge light and the residuals to the disc model. We model the bulge with elliptical isophotes with an axis ratio $b/a = 0.6$ (Ciardullo et al. 1987). We again transform the spatial positions of each point within the bulge to the semimajor axis of the ellipse on which that point lies. We produced the following bulge model using a standard $r^{1/4}$ law (de Vaucouleurs 1948, 1953):

$$\log\left[f_{\rm b}(a_{\rm b})/f_{\rm b}^0\right] = -3.33\left[\left(a_{\rm b}/a_{\rm b}^0\right)^{1/4} - 1\right], \tag{14}$$

where $f_{\rm b}(a_{\rm d})$ is the bulge flux at a position within the bulge with semimajor axis $a_{\rm b}$. A fit is performed to the bulge flux data for $a_{\rm b} \leqslant 15$ arcmin, so that the fit is not influenced by the disc fit residuals. The best-fitting values are $f_{\rm b}^0 = 6\ 914$ adu pixel^{-1} and $a_{\rm b}^0 = 5.1$ arcmin. A plot of the M31 surface brightness against disc semimajor axis distance compared with our model of the surface brightness is shown in Fig. 5.

Our calculation of the bulge and disc scalelengths compare very favourably with those of Irwin et al. (2005) who find a bulge scalelength of 1.4 kpc and an exponential scalelength (disc) of 13.7 kpc, approximately equivalent to angular sizes of ∼6 and ∼60 arcmin, respectively. We note that Pritchet & van den Bergh (1994) also reported a bulge scalelength of 1.3 kpc.

6.2 Testing the distributions

By employing the detection probability function (equation 12) we are able to test three special cases of the CN distribution in M31, namely that novae follow: the overall galactic light, the bulge light only or the disc light only. We use the Kolmogorov–Smirnov (K–S) test in all three cases to ask whether the nova distribution detected is consistent with being drawn from each of the three eruption distributions.

For the bulge-only model, we use the K–S test to determine whether the flux model and the CN distribution are drawn from the same parent population. The upper left plot in Fig. 6 shows the cumulative distribution of bulge detection probability with increasing disc semimajor axis ($a_{\rm d}$) compared with the cumulative detected

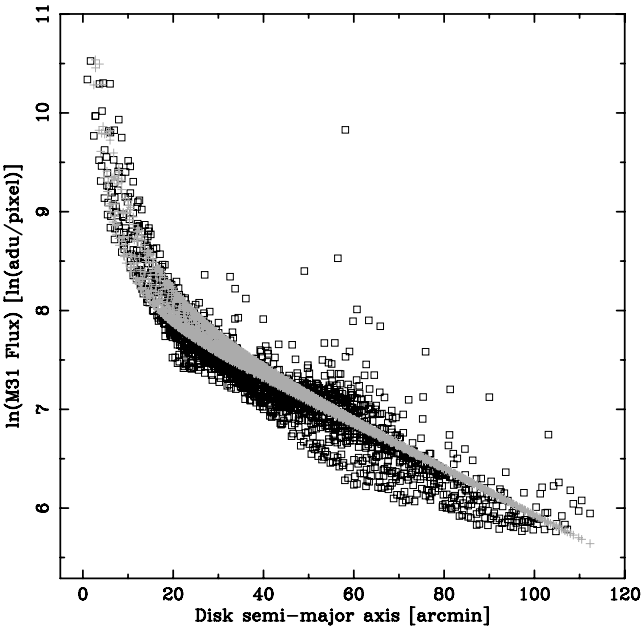

Figure 5. A plot of M31 flux against disc semimajor axis distance. The black squares represent the flux contained within each 1-arcmin cell of the POINT–AGAPE data, plotted with their equivalent disc position. The grey points represent the M31 model flux evaluated for each POINT–AGAPE cell, again plotted with their disc position. The contribution to the overall galactic light from M32 can be seen at around $a_{\rm d} = 60$ arcmin and some structure – mainly from the dust lanes – can be seen within the disc across most of the outer galaxy.

CN distribution with increasing disc semimajor axis. The K–S test produces a probability that the two distributions are drawn from the same parent population of 0.43. Hence, it is clear that the bulge alone can give rise to the observed distribution of CNe.

Next, we test the disc-only model. The upper right plot in Fig. 6 shows the cumulative distribution of disc detection probability with increasing disc semimajor axis ($a_{\rm d}$) compared with the cumulative detected CN distribution with increasing disc semimajor axis. The probability that these two distributions are drawn from the same population is 4.2×10^{-6}. It is therefore quite clear that the disc alone cannot account for the observed distribution of CNe.

Finally, we test the galactic light model. The lower left plot in Fig. 6 shows the cumulative distribution of nova detection probability with increasing disc semimajor axis ($a_{\rm d}$), again compared with the cumulative detected novae distribution with increasing disc position. There is a probability of 1.2×10^{-3} that these distributions are drawn from the same population.

From the results of these tests it is clear that the bulge-only model does a good job of reproducing the observed CN distribution, whilst the disc-only and galactic light models do poor jobs. However, given that the bulge-model overestimates the nova distribution near the centre of M31, where the bulge dominates (see Fig. 6, upper left plot), it is clear that a combination of both bulge and disc populations, with different weightings, is required to adequately model the detected CN distribution.

6.3 The two-population model

Following the results of the testing of the three special case CN eruption models, it seems clear that the favoured model may comprise of a combination of both disc and bulge populations, with each population having a different eruption rate per unit r' flux. To test this new model, we first make the assumption that the nova eruption probability in the disc or the bulge is proportional to the disc or bulge luminosity, respectively:

$$p_i \propto \sigma_{\rm d}\, f_i^{\rm d} + \sigma_{\rm b}\, f_i^{\rm b}, \tag{15}$$

where the disc flux, $f^{\rm d}$, and the bulge flux, $f^{\rm b}$, are defined in equations (13) and (14), respectively, and $\sigma_{\rm d}$ and $\sigma_{\rm b}$ are the number of CN eruptions per unit time per unit r' flux for the disc and bulge populations, respectively.

In order to test this new hypothesis we define the probability of detecting a CN in a particular cell, given that a CN both erupts and is detected within one of the two POINT–AGAPE fields:

$$P_i = \frac{\left(\theta\, f_i^{\rm d} + f_i^{\rm b}\right)\varepsilon_i}{\theta \sum_{j=1}^{N_{\rm bins}} f_j^{\rm d}\,\varepsilon_j + \sum_{j=1}^{N_{\rm bins}} f_j^{\rm b}\,\varepsilon_j}, \tag{16}$$

where θ is the ratio of disc and bulge population eruption rates per unit r' flux.

In order to constrain the favoured value of θ, we employ a maximum likelihood test. The likelihood function chosen is shown in equation (17) below. This function is derived from a simple Poisson analysis of our nova detection model, for a given underlying mean number of expected detections, evaluated over all possible underlying means.

$$P_{\rm model} = \int_0^\infty \frac{\mu^N}{N!}{\rm e}^{-\mu} \prod_{i=1}^{N_{\rm bins}} \lambda_i(\mu)^{n_i}\,{\rm e}^{-\lambda_i(\mu)}\,{\rm d}\mu, \tag{17}$$

where μ is the underlying mean number of expected detections, N is the total number of CN detected by the POINT–AGAPE survey (20), n_i is the number of CN detected in each data bin and $\lambda_i(\mu)$ is the expected number of CN detected in each bin, given by

$$\lambda_i(\mu) = \mu\, \frac{\left(\theta\, f_i^{\rm d} + f_i^{\rm b}\right)\varepsilon_i}{\theta \sum_{j=1}^{N_{\rm bins}} f_j^{\rm d}\,\varepsilon_j + \sum_{j=1}^{N_{\rm bins}} f_j^{\rm b}\,\varepsilon_j}. \tag{18}$$

In order to confine the range over which the likelihood function is investigated we change variables from θ to the bulge fraction (Φ), where Φ is defined as the fraction of the eruption probability within the POINT–AGAPE field due to the M31 bulge:

$$\theta = \frac{1-\Phi}{\Phi}\,\frac{\sum_{j=1}^{N_{\rm bins}} f_j^{\rm b}}{\sum_{j=1}^{N_{\rm bins}} f_j^{\rm d}}. \tag{19}$$

Fig. 7 shows a plot of the normalized likelihood function over a large range of disc/bulge ratios. By evaluating the distribution of the likelihood function, we derive the most likely value of $\Phi = 0.67$ and, by assuming a linear prior in Φ, we evaluate confidence limits about the most likely value. As such, we find that the 95 per cent confidence interval of Φ is

$$0.46 \leqslant \Phi \leqslant 0.82. \tag{20}$$

Using equation (19), this equates to a favoured value of $\theta = 0.18$ with the 95 per cent confidence interval bounded by $\theta = 0.91$ and $\theta = 0.02$. This result also allows us to rule out models with $\sigma_{\rm d} \geqslant \sigma_{\rm b}$ at the 95 per cent level, lending strong support to the existence of separate bulge and disc CN populations.

The maximum likelihood analysis was also simply extended to allow for the uncertainty in the four parameters used to define the M31 surface brightness model (see equations 13 and 14). However, it was found that any small variation in these parameters had a negligible effect upon the favoured value of θ and its associated uncertainty.

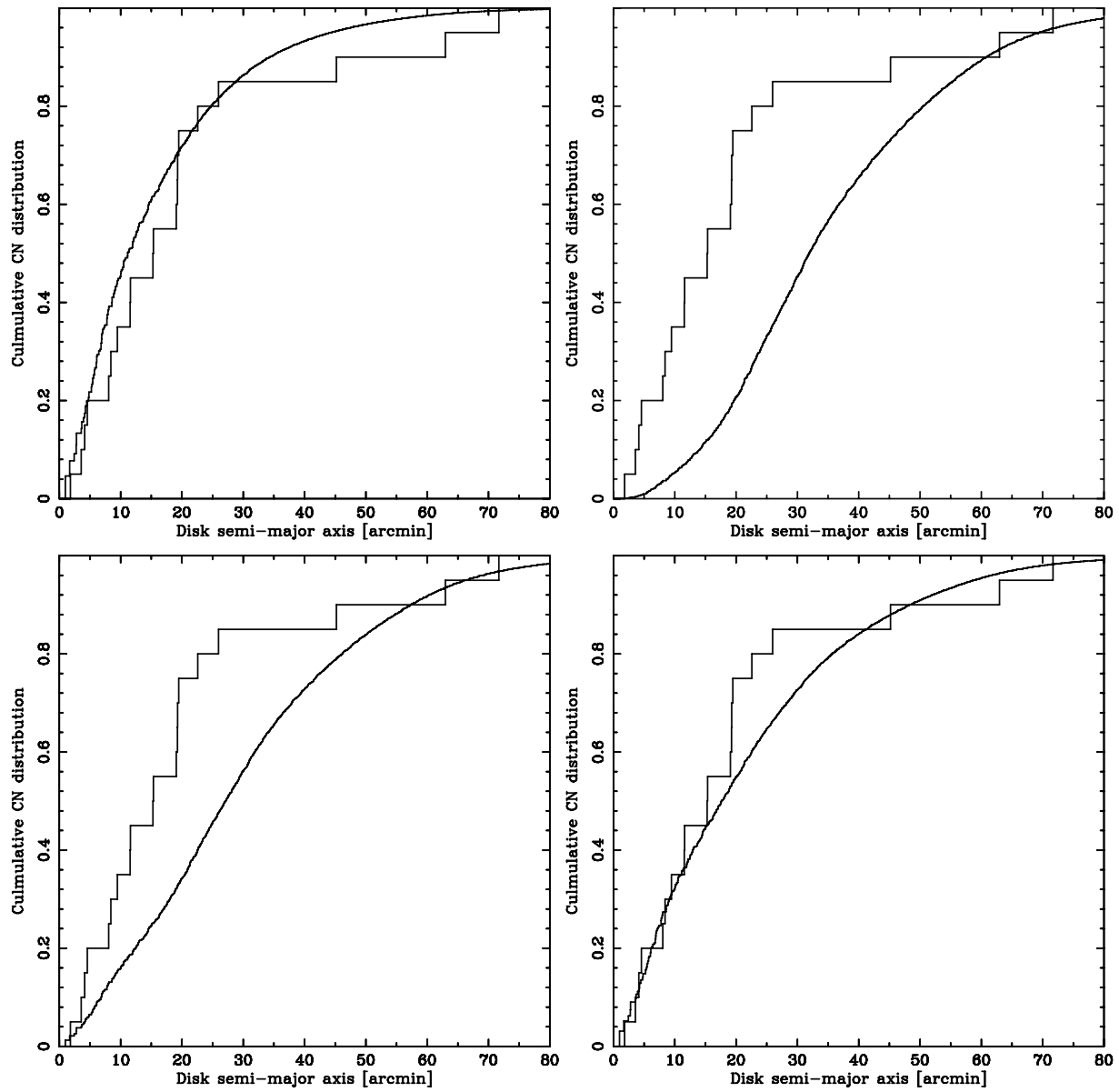

Figure 6. The major axis distribution of the 20 detected POINT–AGAPE novae (grey histograms) along with theoretical predictions of four models (black lines). The upper left panel shows the bulge-only model, whilst the upper right panel shows the disc-only model. The lower left panel shows the galactic light model, whereas the lower right panel represents the most probable distribution (see Section 6.3).

7 M31 CN RATE

The CN eruption probability model is used, in conjunction with the detection completeness data, to compute an estimate of the global nova rate in M31. The total number of CNe observed within the POINT–AGAPE fields must be proportional to the total probability of detecting a CN within those fields, so we have

$$\xi \sum_{i=1}^{N_{\rm bins}} \varepsilon_i \, \Psi_i = n, \tag{21}$$

where ε_i is the probability of detecting an erupting CN at a particular location, Ψ_i is the probability of a CN erupting at that location, n is the number of novae detected within the POINT–AGAPE data set (20) and ξ is an unknown constant relating the detection probability to the recovered number of novae. The definition of the eruption probability given in equation (15) is used to define Ψ_i as follows:

$$\Psi_i = \frac{\theta f_i^{\rm d} + f_i^{\rm b}}{\theta \sum_{j=1}^{N_{\rm bins}} f_j^{\rm d} + \sum_{j=1}^{N_{\rm bins}} f_j^{\rm b}}. \tag{22}$$

The value of the multiplier ξ can be computed for a number of different values of θ, thus producing a range of M31 nova rates. However, we will restrict the values of θ examined to those that relate to specific physical situations: $\theta = 0$, the bulge-only system; $\theta = 1$, the galactic light scenario; $\theta \to \infty$, the disc-only system and $\theta = 0.18$, the favoured value produced by the maximum likelihood analysis of the two-population model. The computed values of ξ for these models are given in Table 3.

The global M31 CN number can now be computed from

$$N = \frac{\xi}{\varphi}, \tag{23}$$

© 2006 The Authors. Journal compilation © 2006 RAS, MNRAS **369,** 257–271

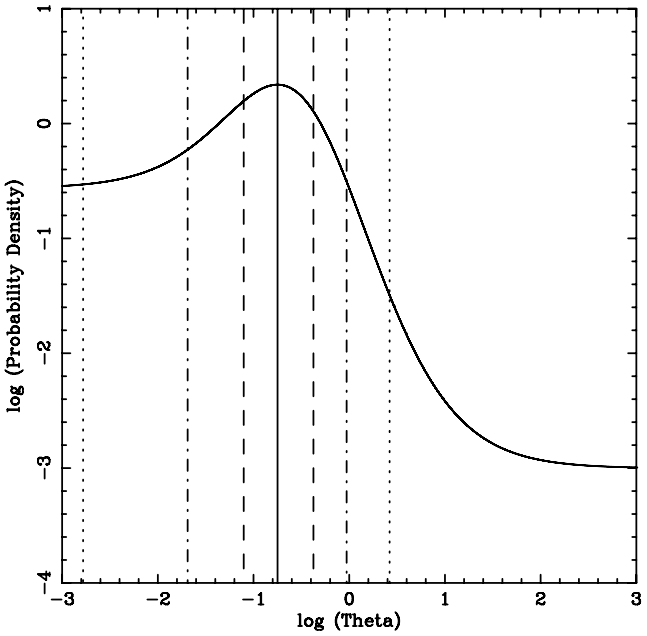

Figure 7. A plot showing the distribution of normalized likelihood probabilities over a large range of disc/bulge ratios. The solid vertical line represents the position of maximum likelihood, the dashed lines represent the 1σ confidence limits, the dot–dashed line the 2σ limits and the dotted lines the 3σ limits.

Table 3. The computed values of the nova rate normalization (ξ), the approximate bulge-to-disc probability ratio, the fraction of novae erupting within the POINT–AGAPE fields (φ), the underlying number of nova eruption (N) during the survey lifetime, the M31 bulge nova rate ($\dot{N}_{\rm bulge}$), the disc nova rate ($\dot{N}_{\rm disc}$) and the global nova rate ($\dot{N}$) for a range of different CN eruption probability models.

θ	ξ	Bulge:disc probability ratio	φ	N	$\dot{N}_{\rm bulge}$ (yr^{-1})	$\dot{N}_{\rm disc}$ (yr^{-1})	$\dot{N}$ (yr^{-1})
0.00	92.61	1:0	0.58	159	56 ± 13	–	56 ± 13
0.18	86.01	4:3	0.47	184	38 ± 8	27 ± 6	65 ± 15
1.00	77.99	1:4	0.37	213	15 ± 3	61 ± 14	75 ± 17
$\rightarrow \infty$	72.73	0:1	0.31	233	–	82 ± 18	82 ± 18

where N is the global nova number and φ is a constant multiplier that accounts for the proportion of the total galactic eruption probability that has been sampled by the POINT–AGAPE survey. φ is defined by

$$\varphi = \frac{\sum_{i=1}^{N_{\rm bins}} \left(\theta f_i^{\rm d} + f_i^{\rm b}\right)}{\sum_i^{M31} \left(\theta f_i^{\rm d} + f_i^{\rm b}\right)}. \quad (24)$$

In order to evaluate the sum over the entire galaxy (the denominator of equation 24), we extend the 1-arcmin grid, initially used to model the completeness, over all space. As galactic discs are known to be truncated radially at a distance of 3–4 scalelengths (van der Kruit & Searle 1981; Pohlen, Dettmar & Lütticke 2000), we evaluated the sum out to a distance of 20 kpc (Ibata et al. 2005) (equivalent to a disc semimajor axis distance of ∼90 arcmin) from the centre of M31. Table 3 shows the computed values of φ for the models tested. We are now able to compute the global number of CNe that erupted in M31 during the POINT–AGAPE observing baseline. These values are also shown in Table 3 for the four model examples.

However, to calculate the global M31 CN rate, we first need to take account of the finite observable lifespan (as defined solely by our observations) of each of the detected novae. As we did not require that a nova's light-curve should be completely contained within our data, our effective baseline for each CN is extended by the lifespan of that particular CN. As the novae have been seeded uniformly over the POINT–AGAPE fields and each seeded nova is selected randomly, the baseline of observations has been extended on average, by the mean lifetime of all 20 novae:

$$T = T_{\rm baseline} + \bar{t}_{\rm nova}, \quad (25)$$

where $T_{\rm baseline}$ is the time between the first and last POINT–AGAPE observation (2.472 yr), and $\bar{t}_{\rm nova}$ is the mean lifetime of the 20 POINT–AGAPE novae (0.359 yr). The effective baseline for CNe of the POINT–AGAPE survey is therefore 2.830 yr. The nova rate for M31 is then

$$\dot{N} = \frac{\xi}{\varphi T}. \quad (26)$$

The computed M31 global CN rates for our four model scenarios are given in Table 3. This illustrates that the predicted overall nova rate is only modestly dependent upon the eruption model chosen. However, the separate bulge and disc novae rates show a strong dependence upon θ, as expected.

The errors shown for the nova rates in Table 3 are generated solely from the Poisson errors related to the size of our nova catalogue. Given the small size of this catalogue, this source of error (∼22 per cent) is expected to dominate over all others. The other main sources of error arise from the completeness calculations, the lack of fast novae in the catalogue, the possible misidentification of novae and the modelling of the surface brightness. In addition, our limited knowledge of the internal extinction of M31 makes it difficult to estimate the errors introduced into the completeness by its exclusion. However, we expect these errors to be small. The maximum r' extinction expected in the disc is ∼0.7 mag; as all the POINT–AGAPE novae were followed through at least one magnitude, it is expected that few, if any, novae were missed due to extinction problems. Should a non-CN have been wrongly included within the nova catalogue, this would directly result in a 5 per cent reduction of the nova rate (see equation 21), coupled, indirectly, with a further maximum decrease of 5 per cent from the completeness model. Hence, the misidentification of a single nova generates a maximum absolute error of ∼7 per cent. However, the errors introduced into the completeness through misidentification are highly likely to be much less than 5 per cent. Likewise, a single CN which is 'missed' due to extinction would induce a maximum increase of ∼7 per cent of the global nova rate. Although there is some error in our modelling of the M31 surface brightness within the POINT–AGAPE fields, the good fit of the model shown in Fig. 5 suggests that this is modest.

Taking the above error discussion into account, we can use the value of $\theta = 0.18^{+0.24}_{-0.10}$ deduced from the likelihood analysis of the two-population model to produce a model constrained estimate of the true nova rate of M31. By evaluating the error on the bulge fraction determination, we are able to show that the Poisson errors are still the dominating error source although there is also a significant contribution from the uncertainty in the model. Hence, we arrive at the following estimate of the true observable nova rate of M31:

$$\dot{N} = 65^{+16}_{-15}\ {\rm yr}^{-1}. \quad (27)$$

8 DISCUSSION AND CONCLUSIONS

8.1 Novae as distance indicators

Sections 3 and 4 report the calibration of both the MMRD and t_{15} relationships using the POINT–AGAPE CN catalogue, which includes a recalibration of each nova's decay rate and assessments of the uncertainties in the maximum light and line of sight extinction to each nova.

The two POINT–AGAPE MMRD relationships (see equations 5 and 6) are consistent with the existence of an MMRD relationship for the r' and i' filters. In fact, the observed scatter in both relationships, although higher than that of recent Galactic calibrations, can be accounted for solely by extinction and maximum light uncertainties. We are able to show that, for the speed classes used for the MMRD calibration, missing the maximum light of a nova by up to a week is not the dominating factor in the MMRD scatter. We also find that for the bright novae for which a linear MMRD is expected, extinction corrections make little difference to the slope determination. However, it is clear that a better understanding of the extinction affecting the POINT–AGAPE novae is required in order to make a more precise calibration of the MMRD within M31. Little more can be said about the comparison between previous MMRD relationship calibrations and the POINT–AGAPE calibrations, as the Galactic MMRD relations (and previous M31 relations) are calibrated using bluer filter bands than the POINT–AGAPE filters. In fact, our calibrations constitute the first attempt to do so using Sloan filters. Given that CNe become bluer as they decline, we would naively expect the POINT–AGAPE r' and i' slopes to be steeper than the Galactic V-band slope, whereas we find that the r' slope is remarkably similar, with the i' slope being much steeper, as expected. However, it should also be noted that the r' filter contains the Hα emission line. As CNe are known to remain bright in Hα long after the visible light-curve has diminished, this may be adversely increasing our measured r' decline times. It is also known that the decline of the Hα emission of a CN is not well correlated with its Hα luminosity at maximum (Ciardullo et al. 1990; Shafter, in preparation). As such, this could potentially detract from the usefulness of any r' MMRD relationship (Shafter, private communication). The OI8446 line, often seen in CN emission spectra (Martin 1989), may also contaminate the results as it lies within the i' filter (Morgan, Ringwald & Prigge 2003).

The MMRD relationship may be used as a tool to measure the relative distance between two populations of novae. However, given that our calibrations are the first to be carried out for the Sloan r' and i' bands, it would be inappropriate to attempt to estimate the M31 distance by comparison with Galactic V- and B-band relationships.

The analysis of the r' and $i't_{15}$ relationships within the POINT–AGAPE catalogue is, like the MMRD relationship, dominated by the extinction uncertainties within the data. However, the extent of the scatter observed in both the r' and i' data cannot be accounted for by the extinction and maximum light uncertainties alone. A comparison of our t_{15} values with those for bluer bands are, however, consistent with a CN becoming bluer following maximum light.

Fig. 3 shows the distribution of t_n scatter, n days after maximum light. This plot clearly indicates that the scatter between the light-curves is large over the entire period sampled. Also, it is clear that there is no evidence of a minimum in the scatter for times around 15 d. The small minima at $\sim$30 d in the r' data and $\sim$35 d for the i' are related to the sampling of the surveys.

To some extent, the t_{15} analysis is limited by the temporal sampling of the POINT–AGAPE survey. Unlike the MMRD relationship that requires good sampling around the peak of the light-curve and some good sampling of the subsequent decline, to test the t_{15} relationship one also requires good sampling of the light-curve specifically at $\sim$15 d after peak. Due to the make up of the survey, the light-curves are generally constructed from short periods of good sampling, followed by regions with no data (see fig. 2 of Paper 1). As such, a relatively large amount of extrapolation is required to estimate each nova's flux between observations. Given the rather erratic behaviour of a typical CN light-curve, the estimation of the errors induced by linearly interpolating over large periods with no data is a far from trivial task. The r' data are again likely to be adversely affected by the Hα emission. We can conclude that the POINT–AGAPE CN catalogue shows no evidence of a t_{15} relationship, nor strong evidence of convergence at another time-scale. We would require nova light-curves with much more uniform sampling than the POINT–AGAPE novae to be able to make a more definitive statement regarding the t_n relationship's overall validity in the r' and i' filters and its potential usefulness.

8.2 Completeness

Overall, the method employed to evaluate the completeness of the POINT–AGAPE CN catalogue generated by the nova pipeline allowed us to obtain a very good understanding of the CN detection efficiency of both the survey and the pipeline. The completeness analysis took into account a variety of possible selection effects which prevent us from detecting novae. These selection effects included the strongly varying surface brightness of M31, the range of morphologies exhibited by CN light-curves and the temporal sampling of the POINT–AGAPE survey.

Until very recently the detection of novae relied solely upon visual detection, often by the 'blinking' of images. Even the most recent surveys (Shafter & Irby 2001, for example) have relied on some visual inspection, particularly to aid in the detection of the faintest novae. The majority of past nova surveys have also relied upon visual inspection of light-curves to determine the likelihood that an object was a CN (e.g Ferrarese et al. 2003). As our pipeline uses much more robust methods and objective selection criteria to both detect and classify potential CNe, we are confident that the completeness of the catalogue is well understood. Whilst the POINT–AGAPE CN catalogue may not be complete,[4] we are none the less able to quantify our completeness.

There were, however, a number of factors that have not been taken into account by the completeness analysis. As was discussed in Section 2, our knowledge of the internal extinction of M31 is limited and these extinction uncertainties have not been built into the completeness computations. Whilst the extinction may be diminishing our ability to detect novae, especially fainter CNe, its relatively small magnitude should not be too troublesome. There are no very fast novae ($t_2 \leqslant 10$ d) within the POINT–AGAPE catalogue.[5] Whilst this may simply be indicative of our small sample size, there may also be additional selection effects – due to the temporal sampling of the POINT–AGAPE survey – that are preventing us from detecting novae of this class. Both of these effects potentially prevent us

[4] A number of CN candidates contained within the POINT–AGAPE data set are known not to be contained within our catalogue (An et al. 2004; Feeney et al. 2005), for reasons we understand (Feeney et al. 2005).

[5] PACN-99-07 has a great uncertainty in its speed class assignment. Although initially classified as a very fast nova, it is thought more likely to be a moderately fast or slow nova.

from observing novae erupting during the survey. Consequently, the computed completeness is likely to be an overestimate. Given the form of the extinction within M31, it is also likely that the completeness has been over estimated to a greater extent within the disc (due to its generally greater extinction) than within the bulge. However, Shafter & Irby (2001) used observations of the planetary nebula population of M31 to conclude that (in Hα) the observed CN population is not significantly affected by extinction. As it is expected that fast novae are more likely to be observed within the disc of a galaxy (see Section 1.4), the probable exclusion of very fast novae from the catalogue again leads us to conclude that, if anything, we have overestimated the completeness and so underestimated the nova rate.

8.3 M31's CNe population

The analysis of the observed CN distribution within M31 allows us to develop a basic model of the underlying CN distribution. Following the separation of the disc and bulge through modelling of the surface brightness, we are able to show that, within the two POINT–AGAPE fields, the observed CN distribution does not follow that of the galactic light. Nor is the observed distribution likely to arise solely from the disc. Although the bulge alone can support the observed distribution, a combination of a bulge and disc population seems required to fully reproduce the observed distribution.

A maximum likelihood analysis of the two-population model (see Section 6.3) indicates that the ratio of the disc and bulge population eruption rates per unit r' flux is 0.18. This result is consistent with previous findings (Ciardullo et al. 1987; Capaccioli et al. 1989; Shafter & Irby 2001) which reported that the M31 novae are primarily associated with the bulge. Shafter & Irby also reported an eruption rate per unit B flux within the bulge of up to an order of magnitude greater than that of the disc. Fig. 8 shows a schematic plot of our 'best' CN eruption model.

The range of bulge-to-disc eruption rate ratios that are consistent with the range of observed CN distributions ($\theta = 0.18^{+0.24}_{-0.10}$) leads

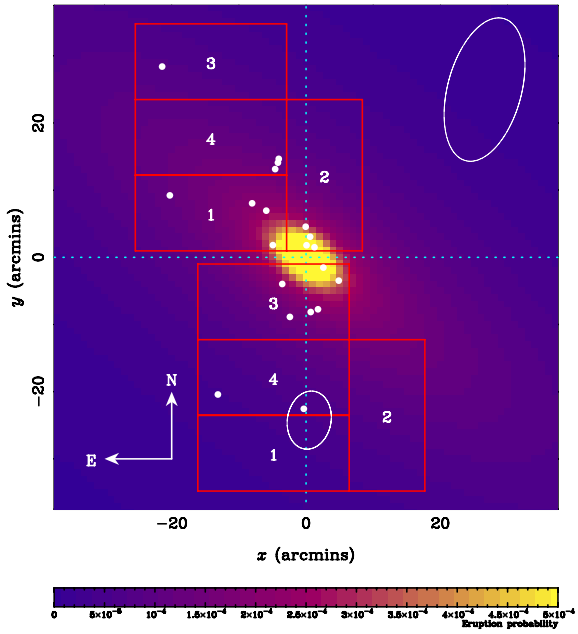

Figure 8. The favoured M31 eruption probability model ($\theta = 0.18$), over plotted with the position of the POINT–AGAPE fields and the 20 detected CNe.

to a range of expected bulge-to-disc nova eruption rate ratios. The global bulge-to-disc CN ratios range from 5 : 1 for a bulge dominant population ($\theta = 0.1$) through to 1 : 4 for the distribution following the surface brightness ($\theta = 1$). The expected nova ratios within the POINT–AGAPE fields themselves range from 20 : 1 ($\theta = 0.1$) to 2 : 1 ($\theta = 1$). However, the POINT–AGAPE survey of M31 covers a much greater surface area of M31 than all previous nova surveys (see Shafter, in preparation, for a summary), which have concentrated mainly on the bulge. The POINT–AGAPE survey has given us much better coverage of the M31 disc and its CN population. As a result, these previous surveys will have all observed a distribution that appears to be much more bulge dominated than that of the POINT–AGAPE catalogue.

The analysis of the M31 CN distribution is, however, limited by a number of considerations. These are mainly the small size of the POINT–AGAPE CN catalogue, the simplistic nature of the M31 surface brightness models and the uncertainties arising from the completeness modelling. Further, the CN distribution analysis relies upon the modelling of the M31 surface brightness. However, this modelling only includes the 'normal' disc component and the bulge component of the surface brightness. Other components, such as the spiral arm structure, the dust lanes (and extinction within M31, in general) and M32, are not taken into account. As with the completeness analysis, these effects are expected to have greater affect within the disc than the bulge. Thus, the inclusion of the dust lanes and spiral structure within the models could lead to an increase in the expected number of disc novae.

8.4 The M31 and Milky Way nova rates

By extending the M31 CN eruption model over the whole galaxy, we are able to produce an estimate of the global nova rate. The computed global observable nova rate of M31 is 65^{+16}_{-15} yr^{-1}, with a bulge rate of 38^{+15}_{-12} yr^{-1} and a disc rate of 27^{+19}_{-15} yr^{-1}. This result is at the limit of being consistent with that of the most robust previous calibration, which found a global rate of 37^{+12}_{-8} yr^{-1} (Shafter & Irby 2001). However, our results are much higher than all previous results, including the Shafter & Irby determination and those of Hubble (1929) ($\sim$30 yr^{-1}), Arp (1956) (24 ± 4 yr^{-1}) and Capaccioli et al. (1989) (29 ± 4 yr^{-1}). The ratio between the bulge and disc nova rate is also markedly lower than that computed by Shafter & Irby's (from their maximum likelihood analysis of the M31 CN distribution).

Despite its apparent high value, we are confident that our computed nova rate is the most accurate evaluation to date of the nova production rate of M31. Our robust completeness analysis and objective selection criteria lead us to believe that the completeness of previous surveys may have been over estimated. Also, given their bulge-centric nature, many previous surveys are likely to have underestimated the contribution from disc novae. Sources of concern in our estimated rate arise again from the extinction uncertainties and the lack of very fast novae in the catalogue. However, both these factors potentially lead to a further increase in the predicted rate, so we are led to conclude that the true global CNe rate of M31 is higher than was previously thought by around 50 per cent.

We can use our estimated global M31 nova rate, along with our computed eruption rates for the bulge and the disc, to produce an estimate of the global Galactic nova rate. Using a similar method to that outlined in Shafter (2002), we assume a Galactic disc-to-bulge luminosity ratio of $\sim$8 and a Milky Way to M31 luminosity ratio of 2/3. Hence, we compute a global Galactic nova rate of 34^{+15}_{-12} yr^{-1}, with a disc rate of 20^{+14}_{-11} yr^{-1} and a bulge rate of 14^{+6}_{-5} yr^{-1}. These

rates are broadly consistent with other Galactic estimates based on M31 data and with estimates based upon direct observations of Galactic novae (see Shafter 2002, for a summary). This result is in excellent agreement with that found by Shafter (1997) who found, by direct observation of Galactic novae, a global rate of 35 ± 11. This is an independent verification of our result for the M31 rate.

ACKNOWLEDGMENTS

MJD and MW were supported by studentships from the Particle Physics and Astronomy Research Council (PPARC). EK and MFB are supported, respectively, by a PPARC Advanced Fellowship and a PPARC Senior Fellowship. SCN is supported by the Swiss National Science Foundation. JA and YT are supported by the Leverhulme Trust.

The authors are grateful to Chris Collins for useful discussions on the statistical analysis and to Nye Evans for useful advice and suggestions. The authors would also like to thank the anonymous referee for their very helpful and constructive comments.

This work is based on observations made with the Isaac Newton Telescope operated on the island of La Palma by the Isaac Newton Group in the Spanish Observatorio del Roque de los Muchachos of the Instituto de Astrofisica de Canarias.

REFERENCES

An J. H. et al., 2004, ApJ, 601, 845
Arp H. C., 1956, AJ, 61, 15
Bertaud C., 1948, Ann. Astrophys., 11, 3
Buscombe W., de Vaucouleurs G., 1955, Observatory, 75, 170
Capaccioli M., della Valle M., Rosino L., D'Onofrio M., 1989, AJ, 97, 1622
Cassisi S., Iben I. J., Tornambe A., 1998, ApJ, 496, 376
Ciardullo R., Ford H. C., Neill J. D., Jacoby G. H., Shafter A. W., 1987, ApJ, 318, 520
Ciardullo R., Shafter A. W., Ford H. C., Neill J. D., Shara M. M., Tomaney A. B., 1990, ApJ, 356, 472
Cohen J. G., 1985, ApJ, 292, 90
Crane P. C., Dickel J. R., Cowan J. J., 1992, ApJ, 390, L9
Crawford J. A., Kraft R. P., 1956, ApJ, 123, 44
Darnley M. J., 2005, PhD dissertation, Liverpool John Moores Univ.
Darnley M. J. et al., 2004, MNRAS, 353, 571 (Paper 1)
de Vaucouleurs G., 1948, Ann. Astrophys., 11, 247
de Vaucouleurs G., 1953, MNRAS, 113, 134
de Vaucouleurs G., 1958, ApJ, 128, 465
de Vaucouleurs G., 1978, ApJ, 223, 351
della Valle M., Livio M., 1998, ApJ, 506, 818
della Valle M., Bianchini A., Livio M., Orio M., 1992, A&A, 266, 232
Downes R. A., Duerbeck H. W., 2000, AJ, 120, 2007
Duerbeck H. W., 1990, Lecture Notes in Physics, Vol. 369. Springer-Verlag, Berlin, p. 34
Feeney S. M. et al., 2005, AJ, 130, 84
Ferrarese L., Côté P., Jordán A., 2003, ApJ, 599, 1302
Freeman K. C., 1970, ApJ, 160, 811
Gill C. D., O'Brien T. J., 2000, MNRAS, 314, 175
Girardi L., Salaris M., 2001, MNRAS, 323, 109
Hatano K., Branch D., Fisher A., Starrfield S., 1997, ApJ, 487, L45
Holwerda B. W., Gonzalez R. A., Allen R. J., van der Kruit P. C., 2005, AJ, 129, 1396
Hubble E. P., 1929, ApJ, 69, 103
Ibata R., Chapman S., Ferguson A. M. N., Lewis G., Irwin M., Tanvir N., 2005, ApJ, 634, 287
Irwin M. J., Ferguson A. M. N., Ibata R. A., Lewis G. F., Tanvir N. R., 2005, ApJ, 628, L105
Jacoby G. H. et al., 1992, PASP, 104, 599
José J., 2002, in Hernanz M., José J., eds, AIP Conf. Proc. Vol. 637, Classical Nova Explosions Am. Inst. Phys., New York, p. 104
Kerins E. et al., 2001, MNRAS, 323, 13
King A. R., 1989, in Bode M. F., Evans A., eds, Classical novae. Wiley, Chichester, p. 17
Livio M., 1992, ApJ, 393, 516
Martin P. G., 1989, in Bode M. F., Evans A., eds, Classical novae. Wiley, Chichester, p. 93
McLaughlin D. B., 1939, Pop. Astron., 47, 410
McLaughlin D. B., 1945, PASP, 57, 69
Morgan G. E., Ringwald F. A., Prigge J. W., 2003, MNRAS, 344, 521
Pfau W., 1976, A&A, 50, 113
Pohlen M., Dettmar R.-J., Lütticke R., 2000, A&A, 357, L1
Prialnik D., Kovetz A., 1995, ApJ, 445, 789
Prialnik D., Livio M., Shaviv G., Kovetz A., 1982, ApJ, 257, 312
Pritchet C. J., van den Bergh S., 1994, AJ, 107, 1730
Rosino L., 1964, Ann. Astrophys., 27, 498
Rosino L., 1973, A&AS, 9, 347
Schlegel D. J., Finkbeiner D. P., Davis M., 1998, ApJ, 500, 525
Schmidt T., 1957, Z. Astrophys., 41, 182
Shafter A. W. 1997, ApJ, 487, 226
Shafter A. W., 2002, in Hernanz M., José J., eds, AIP Conf. Proc. Vol. 637, Classical Nova Explosions: Am. Inst. Phys., New York, p. 462
Shafter A. W., Irby B. K., 2001, ApJ, 563, 749
Shara M. M., 1981a, ApJ, 243, 926
Shara M. M., 1981b, ApJ, 243, 268
Shara M. M., Prialnik D., Shaviv G., 1980, ApJ, 239, 586
van der Kruit P. C., Searle L., 1981, A&A, 95, 105
Warner B., 1989, in Bode M. F., Evans A., eds, Classical Novae. Wiley, Chichester, p. 1
Warner B., 1995, Cambridge Astrophysics Ser., Cataclysmic Variable Stars. Cambridge Univ. Press, Cambridge, New York
Welch D. L., Madore B. F., McAlary C. W., McLaren R. A., 1986, ApJ, 305, 583
Williams R. E., 1992, AJ, 104, 725

This paper has been typeset from a TEX/LATEX file prepared by the author.